Installed jet at take-off conditions: the effect of the external boundary layer thickness on aerodynamics and aeroacoustics

Fulvio Sartor, Fabien Gand, Thomas Le Garrec

▶ **To cite this version:**

Fulvio Sartor, Fabien Gand, Thomas Le Garrec. Installed jet at take-off conditions: the effect of the external boundary layer thickness on aerodynamics and aeroacoustics. AAAF AERO2019, Mar 2019, Paris, France. ⟨hal-02132778⟩

HAL Id: hal-02132778

https://hal.science/hal-02132778v1

Submitted on 17 May 2019

HAL is a multi-disciplinary open access archive for the deposit and dissemination of scientific research documents, whether they are published or not. The documents may come from teaching and research institutions in France or abroad, or from public or private research centers.

L'archive ouverte pluridisciplinaire **HAL**, est destinée au dépôt et à la diffusion de documents scientifiques de niveau recherche, publiés ou non, émanant des établissements d'enseignement et de recherche français ou étrangers, des laboratoires publics ou privés.

HAL Authorization

Association Aéronautique et Astronautique de France

54th 3AF International Conference on Applied Aerodynamics
25 — 27 March 2019, Paris – France

FP56-2019-sartor

Installed jet at take-off conditions: the effect of the external boundary layer thickness on aerodynamics and aeroacoustics

Fulvio Sartor[(1)], Fabien Gand[(2)] and Thomas Le Garrec[(3)]

[(1)]*ONERA - DAAA/ACI. 8, rue des Vertugadins, 92190 Meudon, France. fulvio.sartor@onera.fr*

[(2)]*ONERA - DAAA/MSAT. 8, rue des Vertugadins, 92190 Meudon, France. fabien.gand@onera.fr*

[(3)]*ONERA - DAAA/SN2A. 29, avenue de la Division Leclerc, 92322 Chtillon, France. thomas.le_garrec@onera.fr*

ABSTRACT

This article will present some preliminary results of the numerical activities carried out at ONERA in the framework of the European Project ADEC, part of Clean Sky 2. A dual-stream nozzle installed under a wing in high-lift condition is considered and the interaction between the jet flow and a flap is investigated. In particular, the work focuses on the effect of the nacelle external boundary layer thickness on the jet flow development. The goal of the study is to perform a comparison between a configuration with a thick boundary layer, presented in this article, and a configuration with a thinner boundary layer, already investigated in a previous paper. The simulations are carried out with the Zonal Detached Eddy Simulation in its automatic mode, which allows the use of the method for industrial applications. A preliminary comparison between the two configurations indicate that only small differences can be observed, which is assumed to be due to the fact that the thinner boundary layer is already quite thick. The analysis of the aerodynamic field of the installed configuration gives insights on the consequences of the jet impinging on the flap and on the shielding effect of the wing on the radiated noise.

1. INTRODUCTION

In the framework of sustainable aviation, Ultra High Bypass Ratio (UHBR) nozzles are considered to decrease the environmental footprint of aircraft. The use of such engines leads to thermal, vibrational and acoustic issues linked to close coupled engine integration. In order to accurately compute jet noise, reliable unsteady approaches are needed to simulate the turbulent mechanisms which generate noise. Large Eddy Simulation has proven to be efficient to do so [1] but this approach is challenging to implement in an industrial framework when dealing with complex geometries for which it does not seem to be reasonable nor relevant to resolve the turbulence production mechanisms in all attached boundary layers. Hybrid RANS/LES methods have been developed to model the attached boundary layers and resolve turbulence in free shear layers. Installed configurations are even more challenging to simulate but some authors have shown encouraging results on very complex configurations [15, 17]. In this study, the Zonal Detached Eddy Simulation (ZDES) [8] is used. This approach has been used with success for different academic and technical configurations [9], including academic jet flows [7, 10], dual-stream nozzles [5, 16] and installed configurations [4]. The paper is organized as follows. First, the test cases and flow conditions are described. The grids and numerical methods are detailed in section 3. The results are then analysed in section 4. Conclusions are drawn in section 5.

2. TEST CASE

The configuration investigated in this paper is depicted in figure 1. It consists in a UHBR engine installed under a wing equipped with a flap. The wing is mounted on a small fuselage, while the engine is suspended under the wing, with the pylon not included in the numerical model. The bypass ratio of the nozzle is around 15. The flow conditions in the nozzle exhaust planes, corresponding to sideline conditions during take-off, are given in table 1.

To simulate take-off conditions, the external flow is set at 90 m/s, therefore a boundary layer develops on the external surface of the nozzle. A first investigation with a thin boundary layer (30 mm, corresponding to 0.13 D, where D is the diameter of the secondary exhaust) has

	Pt/Pamb [·]	Tt [K]	Ideal U [m/s]	Ideal MFR [kg/s]
Core	1.222	764.2	292.6	0.414
Bypass	1.342	325.0	229.3	6.373

Table 1: Flow conditions at nozzle exhaust planes.

been conducted in the European Project JERONIMO and the results have been published in a previous paper [11].

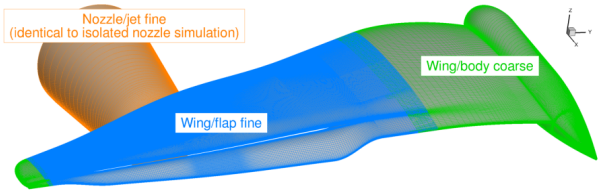

Figure 1: Dual-stream jet installed under a wing with flap: Chimera grid elements.

This work presents the result when considering a thicker boundary layer (65 mm, corresponding to 0.28 D) and some comparison to the case with a thinner boundary layer are also performed. The impact of the boundary layer thickness has already been investigated on the isolated jet configuration by Gand et al. [11]. Those two configurations correspond to two experimental set-up tested in two different wind tunnels.

3. SOLVER

The simulations were performed with the ONERA-Airbus-SAFRAN elsA software, whose developments are partially funded by Airbus, Safran, and ONERA which are co-owners of this software [6]. It solves the compressible Navier-Stokes equations on structured, unstructured and hybrid multi-block grids using finite-volume formulation. For the simulations carried out in this study, the structured capability of the solver is used.

The time integration is performed using an implicit LU-SSOR algorithm and a second-order accurate backward Euler Gear scheme. The number of sub-iterations is adjusted to reach a convergence of one order of magnitude of the inner iteration residuals to achieve second-order time accuracy. For the present simulations, 5 Newton sub-iterations were used. For the spatial integration, the diffusive fluxes discretisation is obtained using a second-order-accurate centred scheme.

The convective terms are treated with a hybrid centred/upwind second-order-accurate modified AUSM+P scheme [13] using a third order MUSCL extrapolation. The use of higher order was not possible due to numerical instabilities on the overset grids and complex geometries. Contrarily to the study with the thinner boundary layer, the AUSM scheme did not involve the *wiggle* sensor to minimize numerical viscosity. The physical time step size is $2.5 \cdot 10^{-7}$ s and the simulated time is 100 ms.

The physical modelling used is the Zonal Detached Eddy Simulation (ZDES) [8], which is a hybrid RANS/LES approach aiming at treating the attached boundary layers in RANS mode and the free shear layers in LES mode. In the present study, the ZDES mode 2 is used, which automatically detects the areas to be treated in RANS (attached boundary layers) and LES (detached flow areas). For the far-field noise computation, the CFD/CAA coupling will be used with the NonReflective Interface approach (NRI) [14]. The results were not available at the time of the writing of the paper, they will be reported in a future communication.

The grid is refined at the walls consistently with the RANS modelling used for the attached boundary layers of the nozzle. The boundary layers are discretised with more than 40 points for the external boundary layer and the first cell center is located at 1 wall unit from the wall. The chimera approach is used to deal with this complex geometry. The chimera assembly is shown in figure 2.

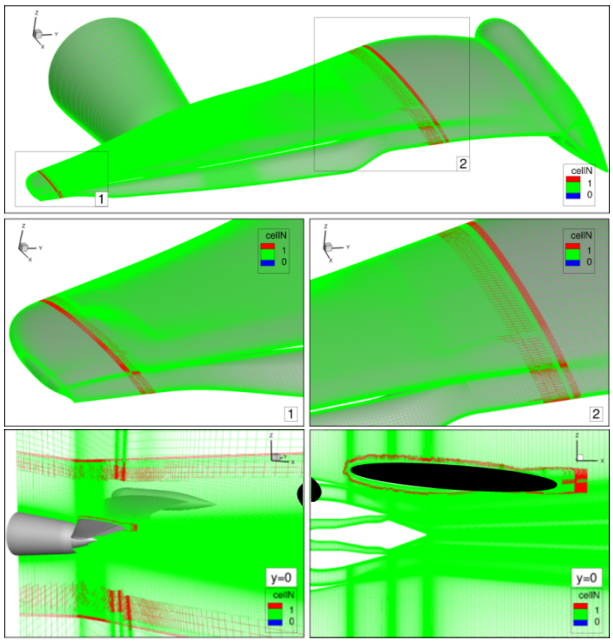

Figure 2: Details of the chimera assembly. Cells in red are interpolated, cells in green are computed.

This meshing strategy also allows to use the exact same grid for the jet as the one used for the isolated nozzle computations, investigated in a previous work [11]. Besides, the grid for the central wing/flap element is refined in the area interacting with the jet. Details of the grid assembly are illustrated in figure 2. The total grid count for the whole configuration is 190 million nodes. The simulation is run in parallel on 756 cores on ONERA cluster, with a CPU cost around $1.2 \cdot 10^6$ hours.

4. RESULTS

This section presents the results of the ZDES simulation: an overview of the results is illustrated in figure 3. The Q-criterion iso-surfaces depicts the coherent structures resolved in the simulation, which are located in the jet and near the flap. One can also observe the lift-induced vortices coming from the flap/wing junctions which are propagated downstream but do not interact with the jet.

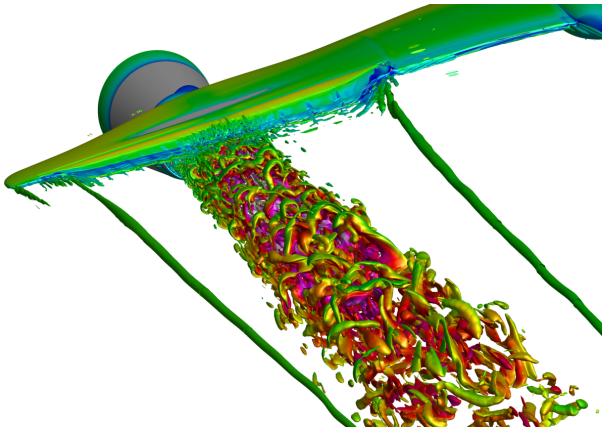

Figure 3: Instantaneous iso-surface of Q-criterion coloured by stream-wise velocity.

Due to the very high by-pass ratio of the engine, the nacelle is closer to the wing than in a classical configuration. Part of the secondary flow exiting from the nozzle is directly impacting the flap, as shown by the turbulent structures of Q-criterion above it. This flap/engine interaction can have a strong impact on the unsteady aerodynamic loading as well as the heating effect due to the high temperature of the jet, as discussed later.

The main focus of this study is the investigation of the installation effect of the jet and the impact of the flap on the flow development downstream of the wing: figure 4 shows the contour map of the turbulent kinetic energy on vertical planes normal to the jet axis, at different locations downstream of the jet. Figure 4a has been obtained with a thinner boundary layer (see [11]), while 4b with the thicker one. In both cases, the asymmetry of the jet and its deformation along the Z axis due to the interaction with the wing and flap is visible thanks to the different contours levels, where higher values of turbulent kinetic energy are observed in the upper part of the jet due to mixing with the flap wake.

When comparing figure 4a with figure 4b, starting from the position closer to the nozzle exit (top of the image), it is clear that the two configurations present different boundary layer thickness. Focussing on $x/D = 3.0$, important differences can be observed in terms of uniformity of the jet: when the boundary layer is thinner, the highest values of turbulent kinetic energy k are located on the upper side of the jet (close to the flap), with values up to twice as big as the values on the bottom. On the contrary, when considering the case with a thicker boundary layer (figure 4b, on the right), the jet is more uniform, even if k is still higher in the region closer to the flap. When moving further downstream ($x/D = 5.0$), this behaviour is still present, while in the $x/D = 10.0$ plane the two configurations are almost identical. In all plane locations downstream $x/D = 1.0$, one can observe that the jet is not larger when the boundary layer is thicker, suggesting that primary effect of the boundary-layer thickness is on the development of the mixing layer downstream of the wing.

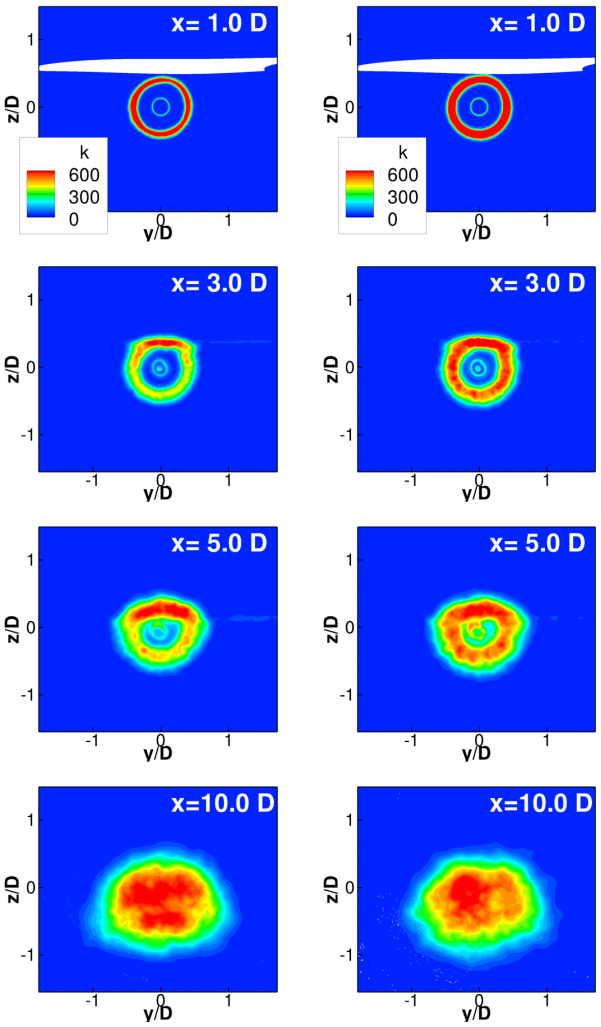

(a) Thin boundary layer (b) Thick boundary layer

Figure 4: Time-averaged resolved turbulent kinetic energy fields (k) at different stream-wise locations.

Figure 5a and 5b represent a vertical slice ($\theta = 0°$) coloured by the pressure fluctuations. They illustrate the jet flow development and interaction with the wing and flap. As expected, the jet is deviated in the $\theta = 0°$ plane due to the presence of the lifting wing. The figure also

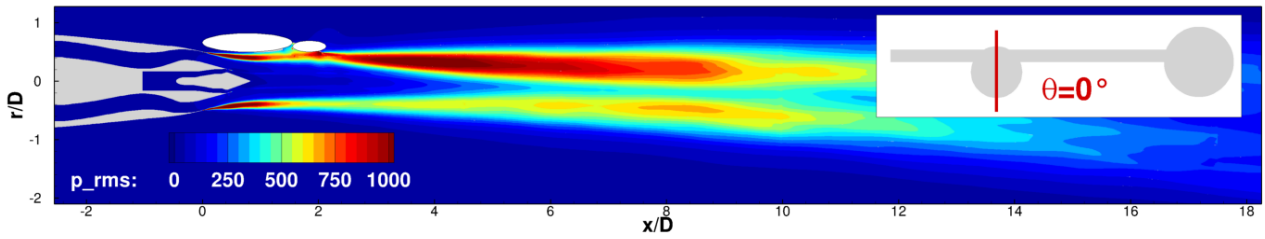

(a) Thin boundary layer, $\theta = 0°$

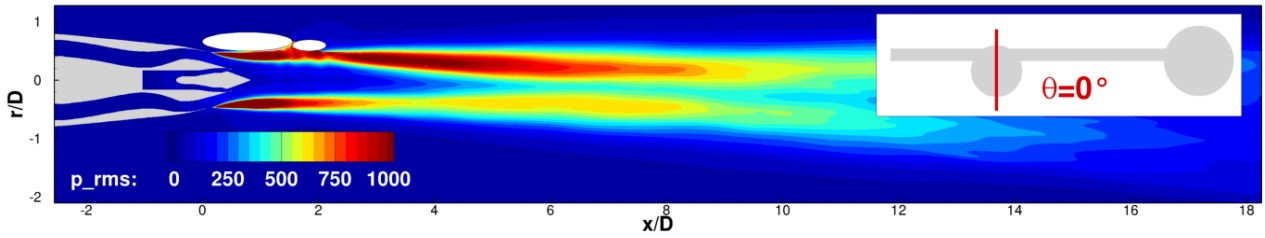

(b) Thick boundary layer, $\theta = 0°$

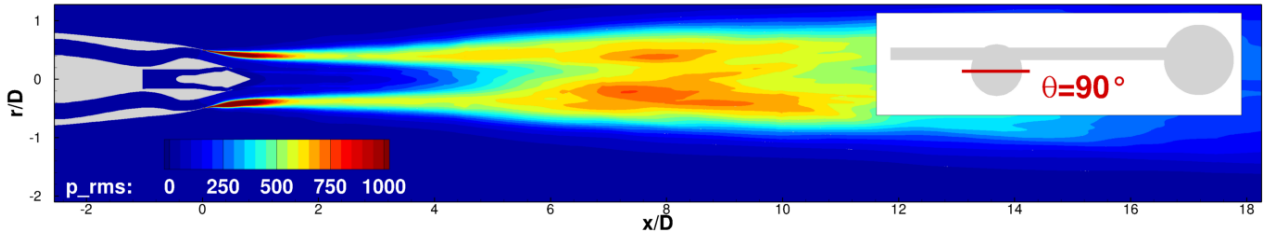

(c) Thin boundary layer, $\theta = 90°$

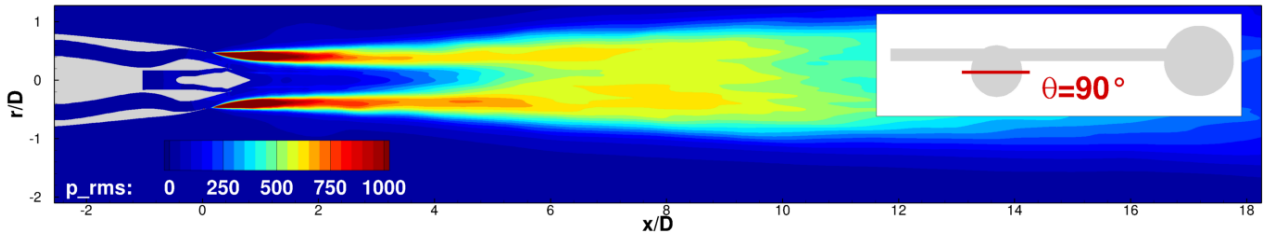

(d) Thick boundary layer, $\theta = 90°$

Figure 5: Time-averaged pressure fluctuations in the vertical plane ($\theta = 0°$) and in the horizontal plane ($\theta = 90°$).

presents a comparison to the result obtained when considering the configuration with a thinner boundary layer. Overall, the potential core is shorten when the boundary layer is thicker (figure 5b), probably because of the larger mixing layer just downstream of the nacelle. This feature has also been observed in the isolated jet configuration, investigated in [11].

The flow deviation in the vertical direction is very similar in the two configurations. The main difference between the two cases is in the flap region: in the case with a thin boundary layer (figure 5a), the mixing layer is also thin, and the region of the flow with high pressure fluctuations does not directly impact on the leading edge of the flap. In the case with a thick boundary layer, the mixing layer downstream of the nacelle hits the pressure side of the wing, and a zone with very high pressure fluctuations impact the leading edge of the flap. In a region around $x/D = 1.5$ and and $r/D = 0.8$ one can see that the flap is in the wake of the mixing layer. This can have a strong impact on the unsteady loads on the flaps and is probably the reason why turbulent structures are visible on the upper side of the wing in the Q-criterion visualisation of figure 3.

Similarly to figure 5a and 5b, figure 5c and 5d present a comparison of pressure fluctuations between the configurations with thin and thick boundary layers, but now focussing on a horizontal plane, corresponding to $\theta = 90°$. The shortening of the jet when increasing the boundary-layer thickness is visible as in the vertical plane. High levels of pressure fluctuations are observed near the noz-

zle exit in the shear layers, which seems to be related to the activation of the resolved turbulent content (the attached boundary layers inside the nozzle are treated in RANS, thus the shear layers experience a RANS-to-LES transition in the early stages of the development). In figure 5d this switch occurs slightly more downstream than in figure 5c. This could be the consequence of the thicker boundary layer. However, due to numerical instabilities in the case with a thicker boundary layer, the numerical scheme is more dissipative in this second case, so the difference could be due to the presence of artificial viscosity.

This behaviour can have an impact on the vortex pairing occurring very close to the trailing edge, during the transition from the attached boundary layers modelled in RANS to the developed shear layers resolved in LES. This phenomenon is known to have consequences on the radiated noise [3, 2, 12], which will be investigated in a future work.

Finally, focussing on the region around $x/D = 8$, the comparison between figure 5c and 5d shows significant differences in the pressure fluctuations downstream of the jet. In the case of a thick boundary layer (figure 5d), the pressure fluctuations decrease monotonically from the shear layer downstream of the nozzle trailing edge. In the configuration with a thin boundary layer (figure 5c) one can observe a region with high pressure fluctuations just downstream of the potential core. This feature can also be related to the slightly higher values of turbulent kinetic energy in the time-averaged results of figure 4, when looking at the bottom figure, referred to $x/D = 10.0$.

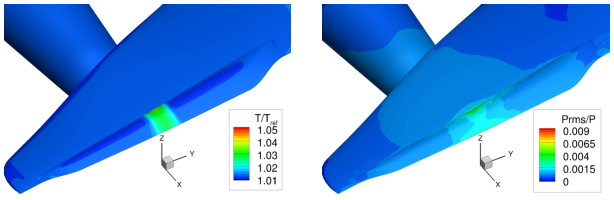

(a) Temperature, upper side (b) Pressure RMS, upper side

(c) Temperature, lower side (d) Pressure RMS, lower side

Figure 6: Average temperature and pressure fluctuations on the walls with the thick boundary layer.

Concerning the interaction between the wing and flap, the average temperature and root mean square (RMS) of pressure can be computed from the time-accurate simulations. The distribution on the upper and lower side are presented on the top and bottom of figure 6, respectively.

The wall temperature indicates that the upper side of the flap (figure 6a) is leached by the secondary stream of the jet which goes through the cavity and around the flap, although the temperature difference with the parts of the flap not in contact with the jet is fairly low since the secondary stream is cold. The region of the pressure side of the wing (figure 6c), where the average temperature is high because of the proximity with the hot flow coming from the core stream, is much larger and extends not only to the flap but also on the wing.

Pressure fluctuations on upper part of the wing (figure 6b) are relatively small, while on the lower side of the wing (figure 6d) it can be seen that the unsteady stream is touching not only the flap, but also the pressure side of the entire wing. Very strong pressure fluctuations are visible in the leading and trailing-edge region of the flap, which will result in unsteady loads as well as installation-related noise sources.

In order to compute the radiated noise, a CFD/CAA chaining approach is required for this complex configuration since it is not affordable to compute the acoustic propagation and reflections within the CFD simulation. The CFD simulation was extracted on volumes defined in the CAA grid to feed the CAA simulation as illustrated in figure 7. The conservative variables are stored in the volumes surrounding the jet. The far-field noise will then be computed using a NRI approach [14].

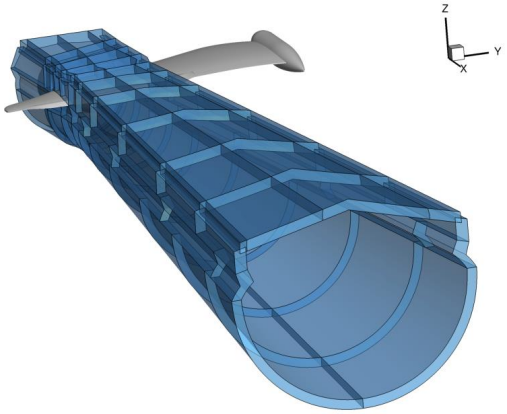

Figure 7: Illustration of the CFD/CAA chaining volumes.

Unfortunately, at the time of the writing of the article the CAA analysis was not available. A future communication devoted to the acoustic analysis of the installation effects will be presented, with a comparison to the configuration with the thinner boundary layer. A similar study has already been published on an the isolated jet configuration by Gand et al. [11].

5. CONCLUSIONS

In this paper, ZDES was used to simulate industrial configurations of an installed jet and evaluate the effect of the external boundary layer thickness. The preliminary results indicate that very small differences can be observed on the aerodynamic properties of the jet when comparing to a previous configuration with a thinner boundary layer on the nacelle. Preliminary acoustic results, not shown in this article, have shown that the presence of the wing entails a shielding effect of the acoustic waves and the near-field fluctuating pressure levels are decreased in the direction above the wing. A CFD/CAA chained simulation will be carried out to further evaluate the noise radiated in this installed configuration with a thick boundary layer.

Acknowledgements

The studies presented in this article have used the ONERA-Airbus-SAFRAN elsA software whose development is partially funded by Airbus, Safran and ONERA, which are co-owners of this software. This project has received funding from the Clean Sky 2 Joint Undertaking under the European Union's Horizon 2020 research and innovation program - ADEC.

REFERENCES

[1] C. Bogey, O. Marsden, and C. Bailly. Influence of initial turbulence level on the flow and sound fields of a subsonic jet at a diameter-based reynolds number of 10e5. *Journal of Fluid Mechanics*, 701:352–385, 2012.

[2] G.A. Brès, F.E. Ham, J.W. Nichols, and S.K. Lele. Nozzle wall modeling in unstructured Large Eddy Simulations for hot supersonic jet predictions. *AIAA paper*, 2013-2142, 2013.

[3] J.E. Bridges and A.K.M.F. Hussain. Roles of initial condition and vortex pairing in jet noise. *Journal of Sound and Vibration*, 17:289–311, 1987.

[4] V. Brunet. Random turbulent flow generation coupled with ZDES for civil aircraft jet configurations. *AIAA paper*, 2012-2896, 2012.

[5] V. Brunet and S. Deck. Zonal Detached Eddy Simulation of a civil aircraft engine jet configuration. *Progress in Hybrid RANS-LES Modelling*, pages 182–191, 2010.

[6] L. Cambier, S. Heib, and S. Plot. The ONERA elsA CFD software: input from research and feedback from industry. *Mechanics and Industry*, 14:159–174, 1 2013.

[7] N. Chauvet, S. Deck, and L. Jacquin. Zonal Detached Eddy Simulation of a controlled propulsive jet. *AIAA Journal*, 45 (10):2458–2473, 2007.

[8] S. Deck. Recent improvements of the Zonal Detached Eddy simulation (ZDES) formulation. *Theoretical and Computational Fluid Dynamics*, 26:523–550, 2012.

[9] S. Deck, F. Gand, V. Brunet, and S. Ben Khelil. High-fidelity simulations of unsteady civil aircraft aerodynamics: stakes and perspectives. application of Zonal Detached Eddy Ssimulation. *Philosophical Transactions of the Royal Society*, 2014.

[10] F. Gand, V. Brunet, and G. Mancel. Zonal Detached Eddy Simulation (ZDES) using turbulent inflow and high order schemes: Application to jet flows. *Notes on Numerical Fluid Mechanics and Multidisciplinary Design*, pages 141–152, 2015.

[11] F. Gand, M. Huet, T. Le Garrec, and F. Cléro. Jet noise of a UHBR nozzle using ZDES: external boundary layer thickness and installation effects. *AIAA paper*, 2017-3526, 2017.

[12] M. Huet. Influence of boundary layers resolution on heated, subsonic, high reynolds number jet flow and noise. *AIAA paper*, 2013-2141, 2013.

[13] I. Mary and P. Sagaut. Large Eddy Simulation of flow around an airfoil near stall. *AIAA Journal*, 40 (6):1139–1145, 2002.

[14] S. Redonnet and G. Cunha. An advanced hybrid method for the acoustic prediction. *Advances in Engineering Software*, 88:30–52, 2015.

[15] J. Tyacke, M. Mahak, and P.G. Tucker. LES of jet flow and noise with internal and external geometry features. *Journal of Fluid Mechanics*, 2015-0503, 2015.

[16] J. Verrière, F. Gand, and S. Deck. Zonal Detached-Eddy Simulations of a dual-stream jet. *AIAA Journal*, 54:3176–3190, 2016.

[17] H. Xia, P.G. Tucker, S. Eastwood, and M. Mahak. The influence of geometry on jet plume development. *Progress in Aerospace Sciences*, 52:56–66, 2012.